ISSN (E): 2959-3921
(P): 2959-393X
DOI: https://doi.org/10.59122/144CFC13

Ethiopian International Journal of Engineering and Technology (EIJET)
Volume 1, Issue 2, 2023

MODELLING FOR MULTIPORT CONVERTER-BASED HYBRID POWER SUPPLY USING RENEWABLE ENERGY SOURCE APPLICATIONS

Yalisho Girma[1*], Dr.Ing.Getachew Biru[2], CS. Reddy[1]

[1]*Adama Science & Technology University (ASTU), Ethiopia*

[2]*Addis Ababa Institute of Technology (AAiT), AAU, Ethiopia*

Corresponding author: *yalishogirma1983@gmail.com*

Abstract

This research work deals with the design and modeling of a multiport converter-based hybrid power supply using solar PV for a small village. The village's maximum power demand is 50kW, consisting of loads in twenty (20) households. The first converter in the proposed multiport system is a high-frequency isolated DC-DC converter fed with an HVDC link yielding an output voltage of 240VDC. The isolated DC-DC converter uses a medium frequency transformer with primary and secondary side converters in an input-series output-parallel (ISOP) configuration. Also, the output of the first converter is connected to a solar PV and battery system through a buck-boost converter. The second converter in the system is a solar PV-fed three-phase modular inverter designed to have an output AC line voltage of 0.415 kV. A solar PV module with an open circuit voltage of 85V and a maximum power rating of 415W is used to feed the inverter. Different scenarios such as changes in load and changes in solar irradiance are used for critically evaluating the performances of the system under question. The output voltage THD, current distortions, changes in the converter output voltage, current magnitude, and converter efficiency are used as performance evaluations of the system under consideration. Simulink/ PLECS (Piecewise Linear Electrical Circuit Simulation) combo simulation platform is used to model and simulate the system in question. Simulation results showed that the proposed multiport converter system can be a viable alternative to a low-frequency distribution transformer.

Keywords: ***Multiport converter, MMC, DC-DC converter, Hybrid power Supply, Solar PV.***

Received: *May 30, 2023;* ***Revised****: 08 October 2023;* ***Accepted:*** *09 October 2023;* ***Published:*** *31 December 2023.*
Corresponding author- ***Yalisho Girma***

I. Introduction

The high carbon emission due to the use of fossil fuel-fired power plants coupled with high environmental concerns in recent times pushed the conventional electric distribution system to integrate more and more renewable energy sources (RES) and modern energy distribution infrastructures. The integration of RES into conventional electric distribution systems requires the active engagement of power electronic converters. The conventional centralized power distribution system uses a low frequency distribution transformer which fails to overcome the extra requirements of present time distribution systems. These extra requirements of today's distribution system include bidirectional power and data flow, easy connection to distributed energy resources, energy storage, load compensation, improved power quality, and reliability.

A multiport power electronic converter-based power supply system can be viewed as an alternative option to a low-frequency transformer to supply both DC and AC loads. In the multiport converter-based power supply system, both DC port and AC port are available, with the function of using distributed energy resources (Solar PV, battery energy system, micro-wind, etc.), AC loads, and DC loads. An isolated DC-DC converter contains a pulse-width modulated inverter at the primary side, a high-frequency transformer, and a PWM secondary rectifier. The input to the isolated DC-DC converter can be an HVDC or modular rectifier connected to the AC grid. The presence of HFT greatly reduces the size and volume of the system to be designed. The modular multilevel inverter is another key element in the multiport converter-based power supply. This component takes a DC input voltage at the output of the DC-DC stage or solar PV and converts it into AC. This component of the multiport converter power supply is a voltage source inverter (VSI) interfaced with low voltage (LV) power distribution systems or loads. It takes a low DC link voltage at its input terminal and converts it into sinusoidal AC voltage having 220 V phase value or 415 V line value, 50Hz specification.

Since LV grid disturbance occurs due to frequent switching in or switching out of heavy loads, output grid filter (common mode and differential mode filter) is required. The use of readily available power switches having low blocking voltage (1.2 kV, 1.7kV, 3.3kV) is a well-established and industrially accepted way for building power processing converter at this stage. This stage also

Received: *May 30, 2023;* ***Revised****: 08 October 2023;* ***Accepted:*** *09 October 2023;* ***Published:*** *31 December 2023.*
Corresponding author- ***Yalisho Girma***

suffers from challenges of high current. To handle the high current demand, interleaved PWM and input series-output parallel (ISOP) converter topologies can be used. The presence of the neutral conductor is also an additional feature required from this stage because the low voltage distribution network is based on Terra-Terra (TT) configuration. The prevalence of load unbalancing and non-linearity, which creates zero sequence current, is another problem that must be properly handled by the three-phase three-wire or three-phase four-wire system. The most appropriate topologies for inverter include a typical two-level voltage source inverter (VSI), a three-level neutral point clamp (NPC), and T-type topologies [1].

However, the two-level or three-level converters are characterized by high conduction loss, switching (turn-on and turn-off) loss, and high dV/dt stress due to the high-frequency operation requirement. For developing highly efficient and reliable inverters, modular inverters based on either Cascaded H-Bridge (CHB) or modular multilevel converter (MMC) having low switching frequency operation can be used. The CHB and MMC-based modular converters have several advantages such as cell and phase modularity, simple voltage and power scaling by combining identical cells, the possibility of using a single capacitor as a means of energy storage for modules, easy bypass of faulty cells during faults (fault ride through capability), low dV/dt, reduced electromagnetic interference (EMI), cost-effectiveness, good transient response, and the possibility of using readily available low voltage power switches. These advantages are obtained at the expense of engaging many passive and active parts as opposed to the non-modular option [2] - [4].

The CHB-based modular inverter requires separate cell voltage, and this may cause complexity in system size and control design. Modular inverter based on MMC topology doesn't need a separate module DC voltage and hence is the focus of this research. A literature survey shows that different PWM techniques have been discussed to operate a modular inverter [2]-[4]. Sub-module capacitor voltage unbalancing is a common problem in MMC and studies conducted [6] have justified the causes of capacitor voltage balancing problems and the strategy to reduce the problem. The input source to the MMC MMC-based modular inverter can be a solar PV battery bank in this research as the location of the project site (Arba Minch) has good solar energy potential as compared with

Received: *May 30, 2023;* ***Revised****: 08 October 2023;* ***Accepted:*** *09 October 2023;* ***Published:*** *31 December 2023.*
Corresponding author- ***Yalisho Girma***

the other RES such as wind. The design and modeling of a multiport converter-based hybrid power supply for the small village (Ayssa Residence) in Arba Minch City is the focus of this study.

The remaining parts of this paper's content are structured as follows: Section two deals with the description of the study area and layout diagram of the proposed system. Section three includes research methodology, a review of the converter configurations, the basic working principles, a mathematical approach to analyzing MMC, multicarrier PWM techniques, solar PV sizing, and the design of buck-boost DC-DC converter. Simulation results and discussion of the proposed system for different scenarios are covered in section four. The last section of the paper is the conclusion.

II. Description of Study Area

The design research is done for Aysa common residents, located in Arba Minch city. The residence is located 7km from the main distribution substation and contains twenty (20) households having a connected load demand of 10kW per household, giving a total of 200kW. Each household has a maximum demand of 4kW and a system maximum demand of 50kW is obtained by considering a diversity factor of 1.6.

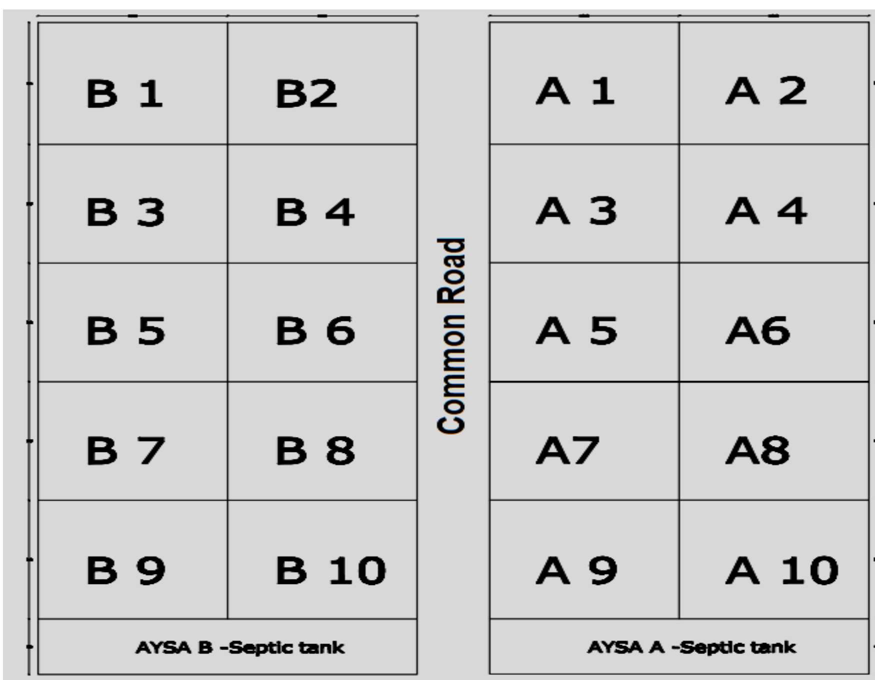

Fig.1. Description of Study Area (codes represent household buildings)

Received: May 30, 2023; **Revised**: 08 October 2023; **Accepted:** 09 October 2023; **Published:** 31 December 2023.
Corresponding author- **Yalisho Girma**

The proposed DC-AC hybrid power supply based on a multiport converter for the village is shown in Fig. 2.

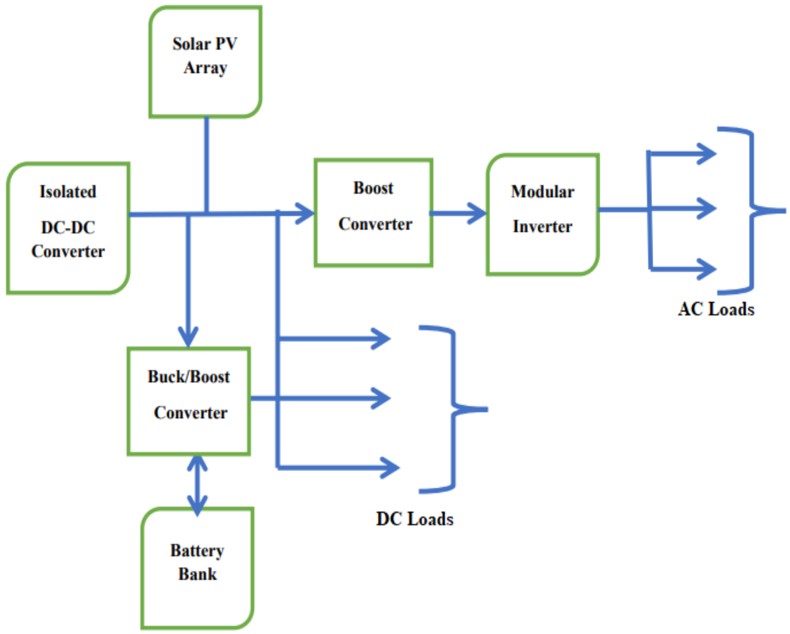

Fig.2. Layout of Proposed Multiport Converter-Based Hybrid Power Supply System

III. Research Methodology

This research work used a modeling and simulation method to evaluate the performances of the various converters. The power circuit and modulation circuit of the system under consideration are modeled in the Simulink/PLECS simulation package and their performance is evaluated for different scenarios such as changes in the load demand and change in the solar irradiance. Performance indicators such as output voltage distortions, current THD, and efficiency (loss) are used. The work presented here is limited to supplying a 50kW load and can be scaled up to handle larger load demand by modifying the number of sub-modules per phase, number of PV modules, and battery.

A. Configuration of Isolated DC-DC Converter

The primary converter of the DC-DC stage takes 24.5kV from the HVDC transmission network. Many candidate topologies such as standard DAB and MAB in symmetrical and asymmetrical configurations can be used. Also, a three-phase DAB can be used in this stage, giving a reduced LV capacitor size. In this research work, the DC-DC stage with symmetrical DAB in ISOP

Received: *May 30, 2023;* ***Revised****: 08 October 2023;* ***Accepted:*** *09 October 2023;* ***Published:*** *31 December 2023.*
Corresponding author- ***Yalisho Girma***

ISSN (E): 2959-3921
(P): 2959-393X
DOI: https://doi.org/10.59122/144CFC13

configuration (Fig.3.1) is to be used in this stage and performance evaluation is made for comparison purposes. The LV DC output voltage of this stage that is fed to the input of the modular inverter is 750V. The selection of transformer type as three-phase or single phase, its shape, core materials, and winding type are contributing factors to the efficient operation of this stage among other factors. This stage operates at high frequency which leads to the reduction of the size of passive components and space requirements. However, high voltage isolation sets an upper limit on the operating frequency of this stage. Due to this, a maximum switching frequency of 20 kHz is recommended to use [19].

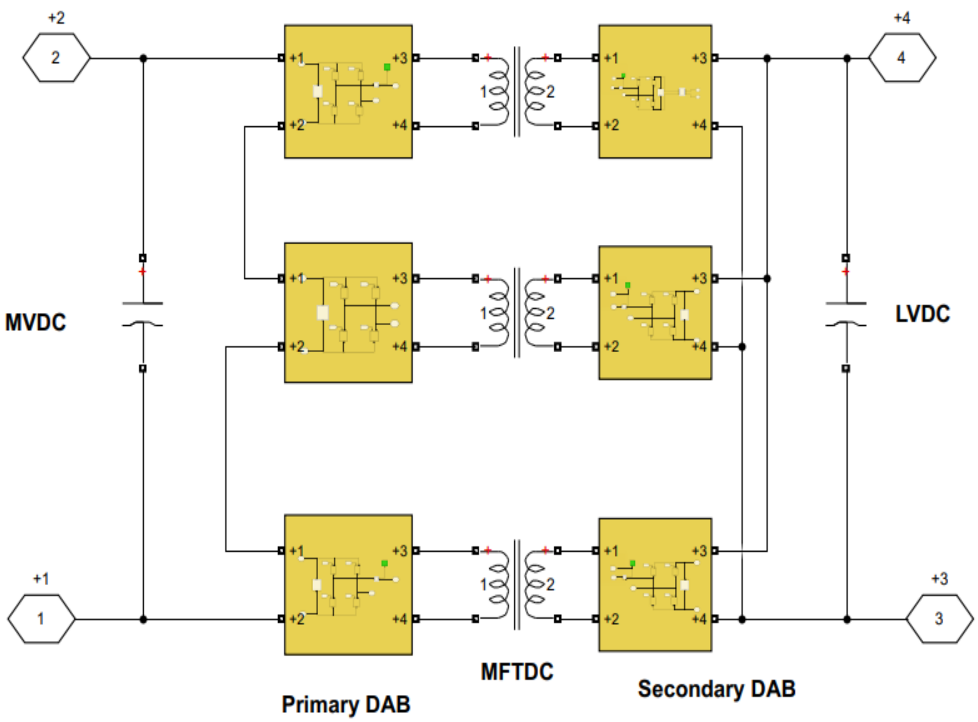

Fig.3.1. Isolated DC-DC Converter in ISOP Configuration

B. Primary and Secondary Side Converter Parameters for Proposed Topologies

As shown in the basic specification Table of the DC-DC stage, the input to the PWM inverter or primary DAB is 24.5kV. For the DAB ISOP configuration shown in Fig. 3.1, the DC link voltage is shared equally in three primary DAB circuits. The peak rectangular AC voltage to each primary DAB should be slightly lower than the DC input to avoid over-modulation. Therefore, a value of 24.5kV/3 = 8.2kV is chosen as the peak AC rectangular voltage for each primary converter. The RMS value of primary DAB is calculated as:

Received: *May 30, 2023;* ***Revised****: 08 October 2023;* ***Accepted:*** *09 October 2023;* ***Published:*** *31 December 2023.*
Corresponding author- ***Yalisho Girma***

$$V_{RMS(P)} = \frac{8.2\text{kV}}{\sqrt{2}} = 5.8\text{kV} \approx 6\text{kV} \qquad (1)$$

Assuming that total power(S) is shared equally among the three primary DABs, the RMS primary currents for the three proposed configurations can be obtained as:

$$I_{RMS(P)} = \frac{S/3}{V_{RMS(P)}} = 2.77\text{A} \approx 3\text{A} \qquad (2)$$

The LVDC requirement as given in basic specification Table 3.2 is 240V because at this stage renewable energy resources such as PV can be interfaced. The MFT output (Secondary side) AC RMS voltage should be slightly less than the output LVDC voltage to avoid over-modulation. If we select a value of 230V, the MFT secondary peak voltage is $230V * \sqrt{2}$ = 325V.

The MFT turn's ratio is given by $\frac{V_P}{V_S}$ = 36:1

In DAB_ISOP configurations, the value of the secondary side current is shared among the parallel-connected secondary DABs as a result of power sharing among the three secondary side converters

$$I_{RMS(S)} = \frac{S/3}{V_{RMS(s)}} = 72.5\text{A} \qquad (3)$$

Based on the above analysis, the semiconductor switch ratings of the primary side and secondary side converters with sufficient consideration of safety factors are summarized in Table.3.3 below.

Table I: Switching Device Parameter for DC-DC Stage

Primary side Voltage = 10Kv					
Device PN and Company	I(A)	Ron (mΩ)	Eon/E-off (mJ)	VG(V)	Configuration
CPM3-10000-0270 (CREE)	20	300	6/1		DAB_ISOP,
Secondary side Voltage = 900V					
Device PN and Company	I(A)	Ron (mΩ)	Eon/Eoff(mJ)	Vf (V)	Configuration
SD11740 (Solitron)	100	8.6	3.5/0.7		DAB_ISOP

Received: May 30, 2023; **Revised**: 08 October 2023; **Accepted:** 09 October 2023; **Published:** 31 December 2023.
Corresponding author- **Yalisho Girma**

C. Configuration of Modular Inverter

The two-level and three-level VSI suffer from high dV/dt, and di/dt and lack intelligent operation (activation and deactivation of modules) in the time of partial loading of the distribution grid. A possible solution to these problems is to use different types of multilevel inverters that utilize low voltage switches and low switching frequencies as discussed in [7]. Many topologies can be used as basic building blocks, but the half-bridge sub-module shown in Fig.3.3 is selected as it has a low switch count and hence low switching and conduction losses.

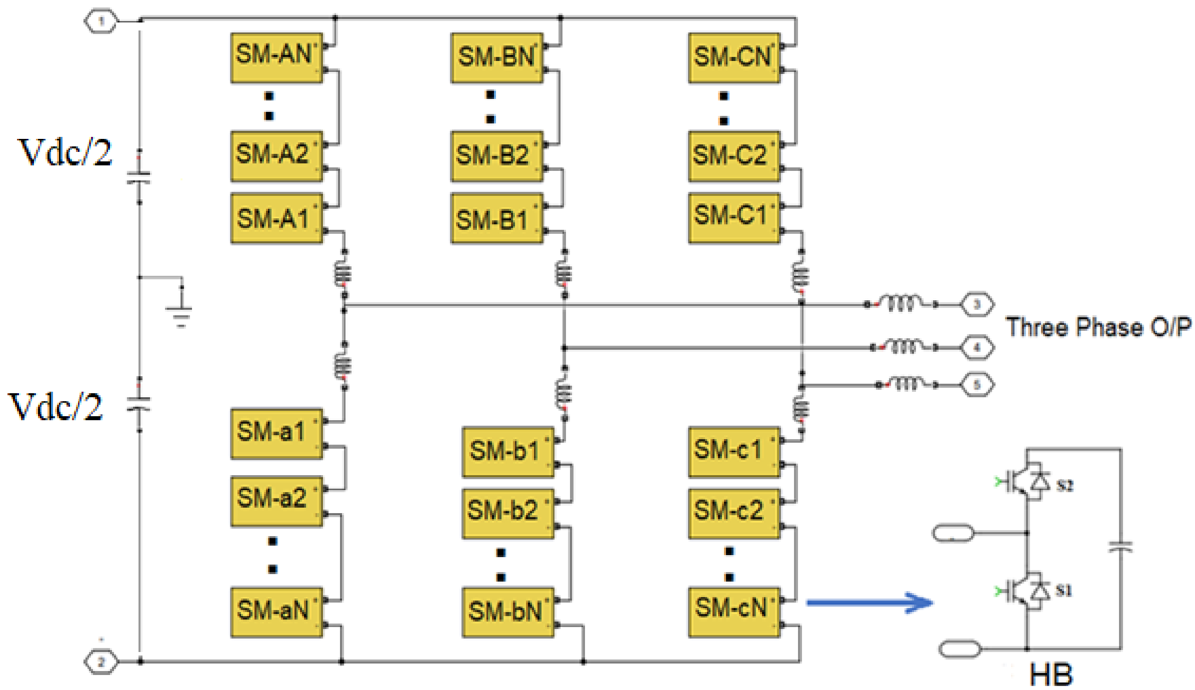

Fig. 3.2. Modular Inverter

The half-bridge sub-module (HBSM) which is used as a basic building block can have four operation states based on the direction of current flow. When current flows into the capacitor or out of the capacitor, the sub-module is said to be in insertion mode, in which case current flows through the upper switch or upper diode. On the other hand, when current flows in the lower switch or lower diode, the sub-module is said to be in bypass mode, in which case the sub-module output voltage is zero.

Received: *May 30, 2023;* ***Revised****: 08 October 2023;* ***Accepted:*** *09 October 2023;* ***Published:*** *31 December 2023.*
Corresponding author- ***Yalisho Girma***

1) Sizing of several sub-modules and passive components: - As shown in Fig.3.2, the MMC-based inverter is made of an N number of series connected sub-modules per phase leg. The phase legs contain arm inductance which limits the circulating current. The number of sub-modules per phase leg arm (N) is given by the equation below [8]: -

$$N \geq \frac{V_{DC}}{\eta V_{CES}} \quad (4)$$

Where, V_{CES} is the semiconductor blocking voltage η is the de-rating factor and V_{DC} is the DC link voltage.
If the DC link voltage at the inverter input terminal is 750V, a MOSFET with a blocking voltage of 200V and a device de-rating factor of 0.909 is used in the above equation, the number of sub-modules per phase leg arm becomes four (4).

Submodule capacitance (C_{SM}) as a function of apparent power, power factor, average capacitor voltage, acceptable ripple, switching frequency, and modulation index and number of sub-module is given as follows [8]: -

$$C_{SM} \geq \frac{S}{3NmV_C^2\varepsilon\omega}\left[1-\left(\frac{mCos\varphi}{2}\right)^2\right]^{\frac{2}{3}} \quad (5)$$

Phase-leg arm inductance is used to filter out circulating current and limit arm current in the event of a fault. Based on the maximum ripples in the circulating current, the arm inductance can be given by the following expression as discussed in [8]: -

$$L_{arm} \geq 0.25\frac{U_{C,MAX}}{Nf_C\Delta i_{L,Max}} \quad (6)$$

, where $U_{C,Max}$ is the maximum voltage of an SM capacitor; $\Delta i_{L,Max}$ is the product of the maximum current ripple and the circulating current, N is the number of sub-modules and f_C is the switching frequency of each SM. It is a good practice to use the maximum current ripple of 15% as mentioned in [9].

The power electronic building block used to implement the back-end converter is selected based on the type of application and maximum load current and voltage requirement. Based on the power distribution system specification, the maximum load current is 70A, and the line-to-line AC

Received: *May 30, 2023;* ***Revised****: 08 October 2023;* ***Accepted:*** *09 October 2023;* ***Published:*** *31 December 2023.*
Corresponding author- ***Yalisho Girma***

ISSN (E): 2959-3921
(P): 2959-393X
DOI: https://doi.org/10.59122/144CFC13
Ethiopian International Journal of Engineering and Technology (EIJET)
Volume 1, Issue 2, 2023

voltage is 415V with a lagging power factor ranging from 0.95 to 1. Therefore, MOSFET having a blocking voltage rating of 200V or greater and a current rating of 130A or greater will be considered by the device manufacturer, international rectifier, Infineon and others. Nine levels (9-level) back-end converter MMC topology is considered for this project work.

After evaluation of the semiconductor device manufacturer's data sheet, the following semiconductor power switch is chosen for simulation purposes:

Table II: Chosen Power Semiconductor Switches for the System

Device part number	Voltage rating (V)	Current rating(A) @25^{0}C	Manufacturer
Power MOSFET (IRFP4668PbF)	200	130	IR

2) Converter power and semiconductor loss: - The input DC power to the converter and output AC power supplied by the converter can be related by:

$$P_{dc} = V_{dc}I_{dC} = P_{ac} + \text{losses} = 0.5m\frac{Vdc}{2}I_{pp}\cos\alpha\ + \text{Losses} \qquad (7)$$

The losses produced in power electronic systems are caused by intrinsic components such as power electronic devices and ohmic resistors (stray resistance). Power electronic devices dissipate losses due to their non-ideal nature. These losses can be grouped into conduction losses, switching losses, and blocking losses. Blocking loss, which is caused by a small leakage current, can be ignored in most analyses without causing much inaccuracy. For power electronic devices integrated with a diode such as the MOSFET with FRD, losses should be individually specified for both the semiconductor switch and diode.

The losses that happen while the MOSFET or FRD is turned on and conducting current are referred to as conduction losses. Conduction power loss is determined by the product of the on-state voltage and the on-state current. However, multiplying the total conduction loss by the duty factor is the requirement in applications where PWM is used. The total conduction loss dissipated by the MOSFET integrated with FRD is given by the following equation.

$$\text{Pcond}(tot) = \text{Pcond}(IGBT) + \text{Pcond}(Diode) \qquad (8)$$

Received: *May 30, 2023;* ***Revised****: 08 October 2023;* ***Accepted:*** *09 October 2023;* ***Published:*** *31 December 2023.*
Corresponding author- ***Yalisho Girma***

$$\text{Pcond(MOSFET)} = \frac{1}{T}\int_{0}^{T}[V_{CE}(t) * I_C(t)]dt \qquad (9)$$

The average conduction loss of IGBT can be computed by the following equation:

$$\text{Pav}(cond) = V_{CE(S)} * I_C * \delta \qquad (10)$$

Where δ refers to the device duty cycle

The transitions of MOSFET and FRD from on-state to off-state and vice versa do not occur instantly which results in switching losses. Both the current flowing through and the voltage across the device during the transition interval are remarkably larger than zero which leads to large instantaneous power losses.

Equations to determine the switching power losses for an IGBT and FRD are given below: -

$$\text{Psw(MOSFET)} = E_{ON} + E_{OFF} * \quad f_{SW} \qquad (11)$$

$$\text{Psw}(FRD) = E_{rec} * \quad f_{SW} \qquad (12)$$

The turn-on energy (Eon), the turn-off energy (Eoff) in the IGBT, and the reverse recovery energy in the FRD (Erec) are functions of collector current, collector voltage, gate resistance, and junction temperature.

Normalization of the switching losses with the conditions provided for any application with the nominal values from the datasheet is essential.

$$\text{Psw}(MOSFET) = \left(\frac{E_{ON} + E_{OFF}}{\pi}\right) * f_{SW} * \frac{I_{pk}}{I_{nom}} * \frac{V_{DC-link}}{V_{nom}} \qquad (13)$$

$$\text{Psw}(FRD) = (E\_rec/\pi) * f\_SW * I\_pk/I\_nom * V\_(DC - link)/V\_nom \qquad (14)$$

From the determination of the switching and conduction losses of IGBT and FRD, it is possible to obtain total loss for determining the efficiency of the system and the junction temperature of the devices.

$$\text{P}(tot) = P_{Cond}(MOSFET) + P_{SW}(MOSFET) + P_{Cond}(FRD) + P_{SW}(FRD) \quad (15)$$

A piecewise linear electronics circuit system (PLECS) uses a lookup table, formula, or a combination of the lookup table and formula approach to determine conduction and switching

Received: *May 30, 2023;* ***Revised****: 08 October 2023;* ***Accepted:*** *09 October 2023;* ***Published:*** *31 December 2023.*
Corresponding author- ***Yalisho Girma***

losses. [10] The lookup approach uses interpolation and extrapolation methods to find the device loss values based on the set of data points taken from the datasheet. The novelty of this research work is justified by the integration of device thermal models and efficiency calculation models of the converter. The thermal implementation model for a single MOSFET integrated with FRD is given in Fig. 3.6 below. For a power electronic system containing multiple switches, the same approach can be used with a common heat sink shared among all semiconductor switch packages. For efficiency calculation of the power electronic system, the periodic average for conduction losses and periodic impulse average for switching losses obtained from probe output is summed up as described in Fig.3.7 [10].

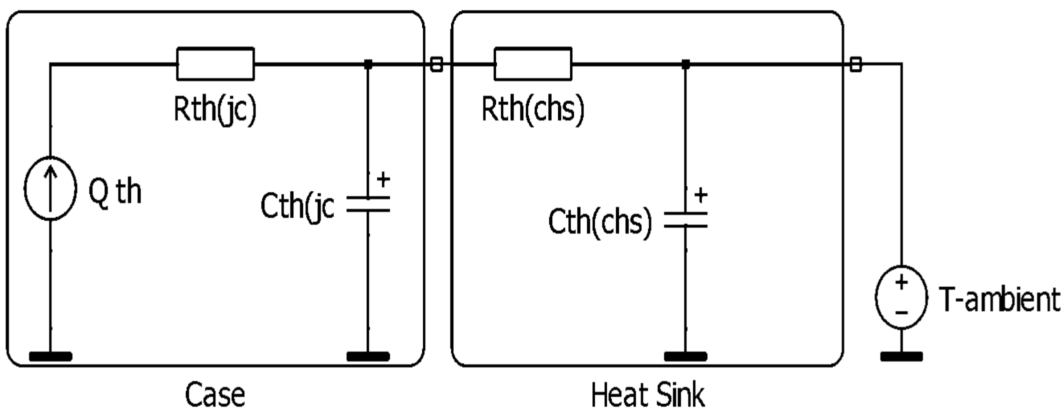

Fig.3.6. Thermal Model of a Single Semiconductor Device

Based on the thermal data collected from the device manufacturer, switching loss and conduction loss are determined by using a look-up table and formula computation method.

The converter efficiency calculation diagram described in Fig.3.7 uses these thermal loss values for calculating the efficiency of the system. The efficiency analysis of the system is done by using the thermal model of the selected silicon carbide power MOSFETs. This is carried out for the MMC converter by using a combination of lookup table and formula for maximum load current and case temperature of 100^0C. All thermal parameters are gathered from the device manufacturer's datasheet [8], [11], [14]. Switching loss, conduction loss and total semiconductor loss of the converter for the selected sub-modules are obtained by using the efficiency calculation model presented in Fig.3.7.

Received: *May 30, 2023;* ***Revised****: 08 October 2023;* ***Accepted:*** *09 October 2023;* ***Published:*** *31 December 2023.*
Corresponding author- ***Yalisho Girma***

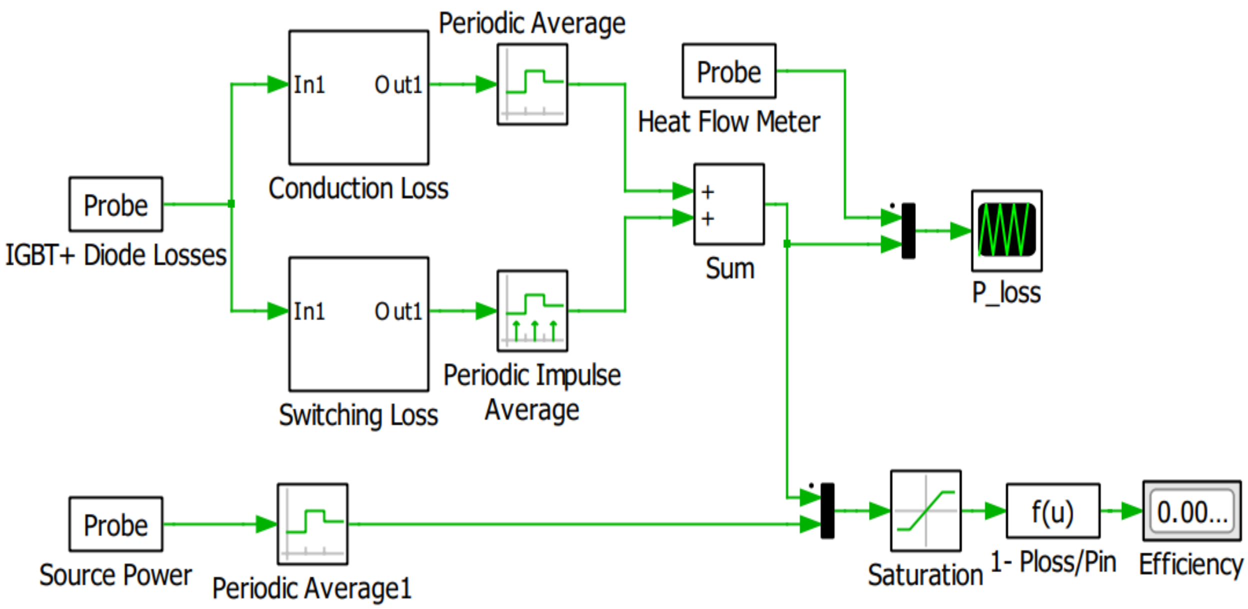

Fig.3.7. Efficiency Calculation Diagram

The converter system efficiency as shown in the model is calculated as follows: -

$$\eta = \frac{P_{out}}{P_{in}} \qquad (16)$$

Expressing P_{out} as a difference of P_{in} and power loss, the above expression is written as

$$\eta = \frac{P_{in} - P_{loss}}{P_{in}} \qquad (17)$$

D. Modulation Method

Many modulation methods such as PSPWM, triangular PWM, and trapezoidal PWM are proposed for isolated-stage DC-DC converters, of which PSPWM is the most widely used one [12]. Among many modulation techniques for MMCs proposed by many researchers, multi-carrier pulse width modulation methods such as level-shifted PWM(LSPWM) and phase-shifted pulse width modulation (PSPWM) are frequently employed for MMC-based modular converters made of low-voltage modules.

In level shift, the PWM distribution of the switching signal is uneven and hence creates uneven switching losses and unbalance of sub-module capacitor voltage. It needs a capacitor balancing

Received: *May 30, 2023;* ***Revised****: 08 October 2023;* ***Accepted:*** *09 October 2023;* ***Published:*** *31 December 2023.*
Corresponding author- ***Yalisho Girma***

algorithm which adds complexity to the modulation circuit as the number of voltage levels increases.

In the case of PS-PWM, the SM capacitor voltage is balanced with a PI controller, and the need to use a sorting algorithm can be avoided. Moreover, the switching signals are evenly distributed in the entire sub-modules, resulting in an equal distribution of switching losses in the converter. The advantage of PS-PWM over LS-PWM is highly observed if the required output voltage level number is large [12]-[14].

To generate the switching signals for a multilevel converter having “N” sub-modules per leg arm, the “N” number of carrier signals is required. The phase difference between consecutive carriers can be found using the equation below:

$$\theta = 360/N \qquad (18)$$

However, to produce an output voltage having 2N+1, the signals between upper arm and lower arm sub-modules have a phase difference given by

$$\theta = \frac{180}{N} \qquad (19)$$

For the implementation of phase-shifted PWM signals, the reference voltage (modulating signal) is compared with a triangular waveform (carrier signal) in a comparator block to determine the switching sequence for the converter. The comparator block yields a high switching signal (1 = switch ON) when the triangular wave is higher than the reference voltage; otherwise, it yields a low signal (0 =switch OFF). The switches in one leg of HBSM and FBSM operate in a complementary manner to avoid short-circuiting. To avoid switching overlap between the upper switch and lower switch in the sub-module, a small dead time (delay time) is added to the PWM signal after the comparator block. The PS-PWM signal generation technique inside the comparator block for two sub-modules (N=2) is demonstrated by the signal diagram in Fig.3.8 [14].

The use of a MMC based back end converter gives a chance to scale up the number of levels in output voltage by a factor of 2 for the same structure, by using interleaved phase shift modulation having π phase angles between the upper and lower arm carriers. This feature of MMC-based BEC gives output voltage with better THD values [15].

Received: *May 30, 2023;* ***Revised****: 08 October 2023;* ***Accepted:*** *09 October 2023;* ***Published:*** *31 December 2023.*
Corresponding author- ***Yalisho Girma***

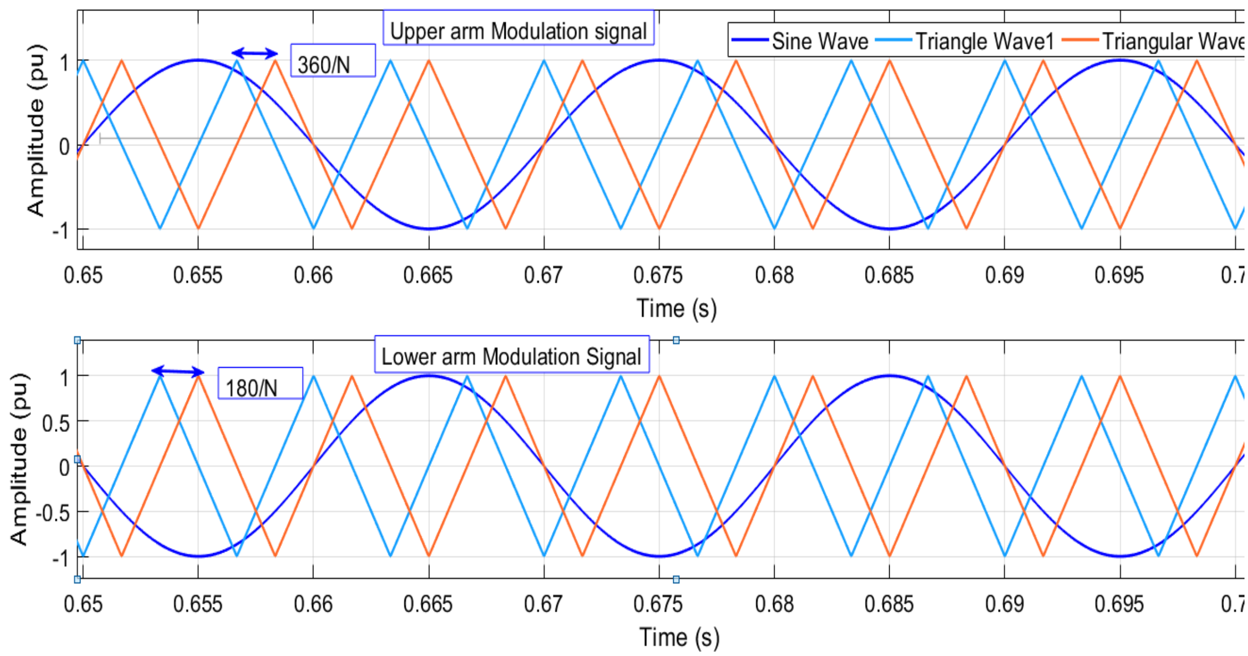

Fig.3.8. Interleaved Phase Shift Modulation

To utilize the above advantage, the interleaved phase modulation technique is applied in this project work.

E. Solar PV Array Sizing

Solar PV as a renewable energy source is drawing much attention in the day-to-day life of the global power industry. This is because of its free, clean, abundant, green nature, and low running cost characteristics. The maximum irradiance at a 15-degree tilt angle in Arba Minch is 2006W/m^2. However, the average global irradiance per day varies between 500 to 1000 W/m^2.

The PV system has two major problems; that is, the conversion efficiency of electric power generation is low and the amount of electric power generated by solar arrays changes continuously because of variations in the insolation due to unpredictable shadows cast by clouds, birds, trees, and so forth. Also, the I-V characteristic of a PV array is nonlinear and varies with irradiation and temperature. The insolation change affects the photon-generated current and has very little effect on the open circuit voltage whereas the temperature variation affects the open circuit voltage and the short circuit current varies very marginally. In general, there is a unique point on the I-V or V-P curve, called the maximum power point (MPP), at which the entire PV system (array, converter,

Received: *May 30, 2023;* ***Revised****: 08 October 2023;* ***Accepted:*** *09 October 2023;* ***Published:*** *31 December 2023.*
Corresponding author- ***Yalisho Girma***

etc.) operates with maximum efficiency and produces its maximum output power. The location of the MPP is not known but can be located, either through calculation models or by search algorithms. However, by incorporating maximum power point tracking (MPPT) algorithms [16], the PV system's power transfer efficiency and reliability can be improved significantly, as it can continuously maintain the operating point of the PV panel at the MPP about that irradiation and temperature. An incremental conductance algorithm is used in the back-boost converter to handle the problem of MPPT**.** This algorithm compares the incremental conductance to the instantaneous conductance in a PV system. Depending on the result, it increases or decreases the voltage until the maximum power point (MPP) is reached. The power-voltage characteristics of Sunpower-SPR-415E-WHT-D PV module at 25^{0}C for different irradiance levels are shown in Figure 3.9.

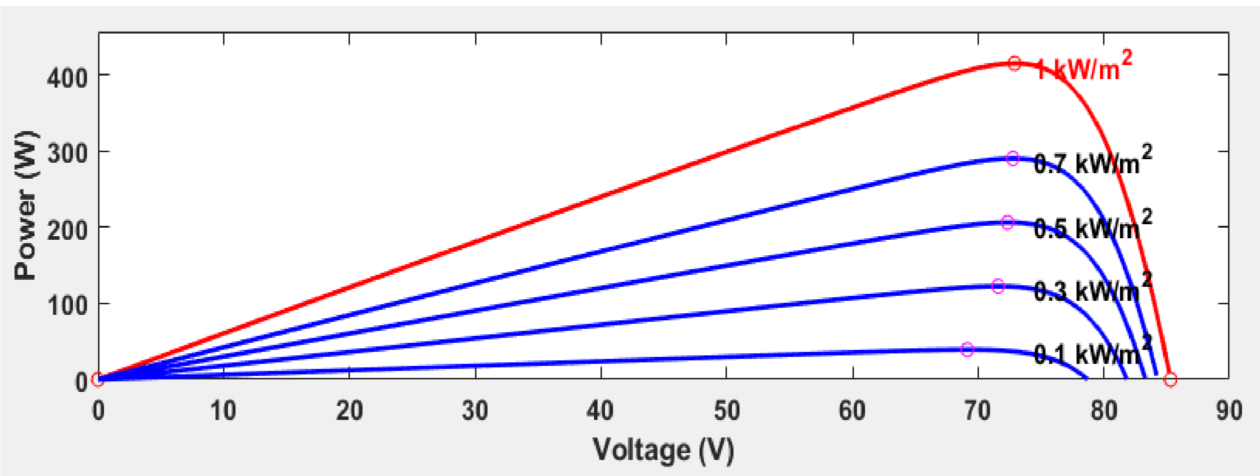

Fig.3.9. P-V Characteristic Curve of Solar PV Module at Different Irradiance.

In this research, a solar PV module (Sunpower-SPR-415E-WHT-D) is used. The module has an open circuit voltage of 85.3V; voltage at maximum power is 73V and it has a maximum power of 414W. The designed system should supply a maximum power demand of 50kW, at 230V (PN). For an MMC-based modular inverter made of four modules, the input DC voltage should be 700V obtained from the output of the boost converter connected to the solar panel to get the 230V (PN) AC. The total number of solar PV modules required to supply the load is the ratio of load power demand to solar module maximum power.

$$\text{No solar modules} = \frac{\text{Load demand}}{\text{Maximum power of Solar PV module} * \eta} \qquad (20)$$

Received: *May 30, 2023;* ***Revised****: 08 October 2023;* ***Accepted:*** *09 October 2023;* ***Published:*** *31 December 2023.*
Corresponding author- ***Yalisho Girma***

If the efficiency of the PV array and that of the buck-boost converter is considered to be 85%, the total number of modules required is 166.

The series connected modules and parallel strings are decided by the total output voltage obtained at the solar PV array i.e., 240V.

$$\text{No of series-connected modules} = \frac{\text{Array output Voltage}}{\text{Module voltage at Maximum power}} \qquad (21)$$

The total DC voltage requirement at the LV DC link is 240V and substitution of this value in the above equation gives the number of series connected modules to be 3.28 ≈ 4**,** which gives the number of parallel module strings to be 42.

F. Battery Sizing

The battery is used as an external energy storage system or agent to sink the power based on the instantaneous load condition. The rates of charging and discharging of the battery are estimated based on the standard specifications of the battery handbook. Lead acid batteries are preferred for standalone applications as their maintenance and the initial costs are less. According to the handbook of the lead acid battery, the charging current of the battery should be less than $0.1CB$, where "CB" is the capacity of the battery in ampere-hour (Ah). For a 200 Ah battery the charging current should not exceed 20 A [Battery Charging Current = 0.1 × 200 = 20A]. Also according to the battery handbook, the discharge current in tens of seconds should not exceed (0.5–0.7) CB and the nominal discharge is $0.1CB$. Here (CB/5) is selected as the maximum discharge current. The sizing of the battery is similar to sizing the solar PV as done before in section 3.5. For a given load power to be delivered by the battery through a boost converter, the maximum capacity can be obtained as given below [17]: -

$$C_B = \frac{P_O}{0.1 * \eta_{Conv} * V_{Bat}} \qquad (22)$$

For a system load power of 50kW, buck-boost converter efficiency of 95%, and battery voltage of 24V, the total capacity of the battery is equal to **21930Ah.** If the selected single lead acid battery has a capacity of **200Ah**, a total of **110** batteries are used to supply the system.

G. Buck-Boost Converter

The output voltage obtained from the solar photovoltaic (PV) panels is very low, and therefore, it cannot be connected to high voltage load or grid directly. Therefore, a non-isolated DC-DC

Received: *May 30, 2023;* ***Revised****: 08 October 2023;* ***Accepted:*** *09 October 2023;* ***Published:*** *31 December 2023.*
Corresponding author- ***Yalisho Girma***

conversion stage with high gain is required to interface the solar PV. The boost converter is placed between the modular inverter and the solar PV so that the output voltage remains fairly constant with variations in solar irradiance. In the absence of solar power, the system gets power from the battery storage system. During normal operation (sufficient solar energy) the battery is charged through the buck-boost converter and stores energy. During night times and cloudy times, the stored battery power supplies the load through the boost converter as in the layout diagram shown in Fig.1. Depending on the charging and discharging condition of the battery sensed, the duty cycle of the buck-boost converter is changed. When the battery is in charging mode, the buck-boost converter operates in buck mode and when the battery is discharged, it operates in boost mode. The Duty cycle in charging mode is 0.12 and 0.90 when the battery is in discharging mode

IV. Simulation Result and Discussion

A. Simulation of Isolated DC-DC stage

The input to this converter is an HVDC transmission network or grid-connected modular rectifier. If the input is obtained from a rectifier connected to the grid having a line voltage of 15kV, a maximum DC voltage of 24.5kV can be obtained, which feeds the isolated DC-DC stage.

Table III: Basic Specification of Isolated DC-DC Converter

Name of Converter	Parameter	Value
	Vin(nominal)	24.5kV DC
	Vout	240V DC
	P_{MAX}	50kW
	Switching frequency	20kHz
	Co	10mF
	Turns ratio	36:1

Received: *May 30, 2023;* ***Revised****: 08 October 2023;* ***Accepted:*** *09 October 2023;* ***Published:*** *31 December 2023.*
Corresponding author- ***Yalisho Girma***

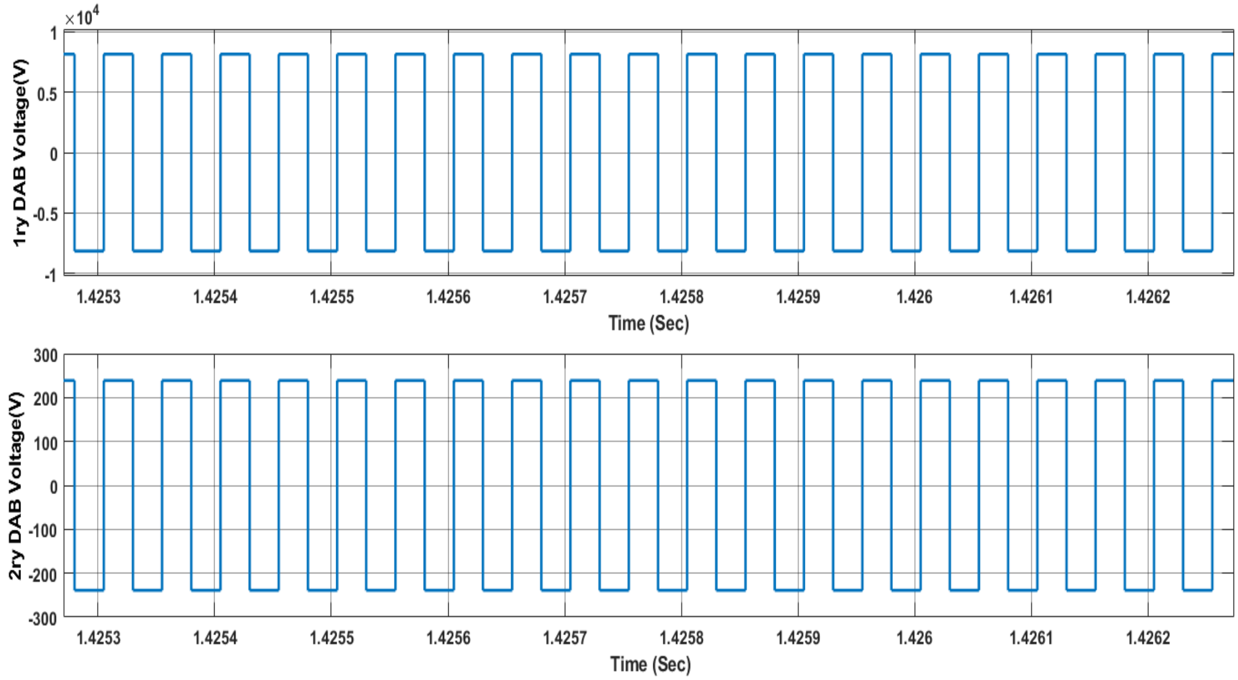

Fig.3.10. Primary and Secondary DAB Voltage

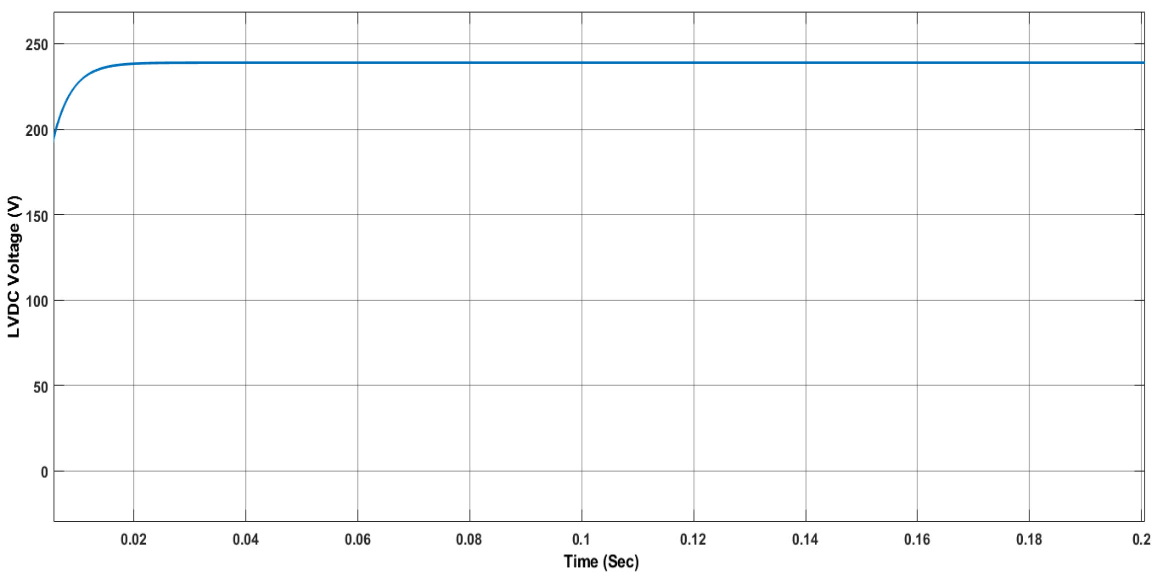

Fig.3.11. LVDC Voltage

Observation: As shown in Fig.3.11 and Fig.3.12, the primary DAB converters share a total input voltage of 24.5kV. Each DAB converter has a value equal to 8kV. Also, the secondary DAB has a peak voltage of 240V.

Received: *May 30, 2023;* ***Revised****: 08 October 2023;* ***Accepted:*** *09 October 2023;* ***Published:*** *31 December 2023.*
Corresponding author- ***Yalisho Girma***

ISSN (E): 2959-3921
(P): 2959-393X
DOI: https://doi.org/10.59122/144CFC13

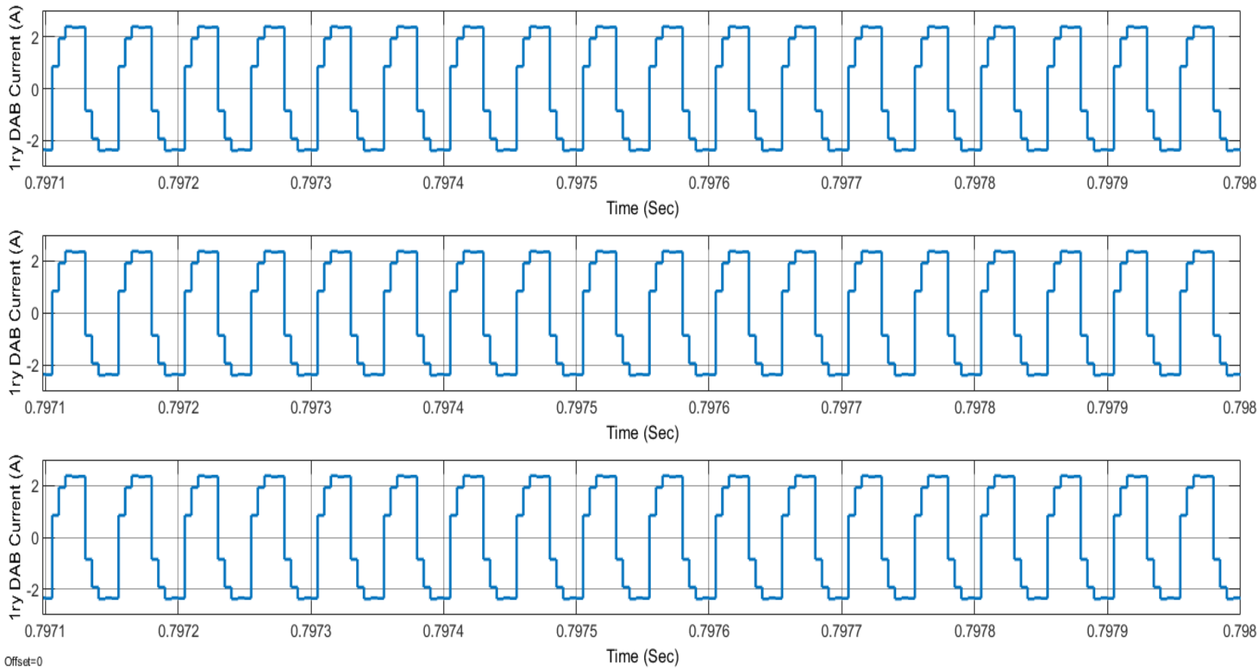

Fig.3.12. Primary DAB Currents

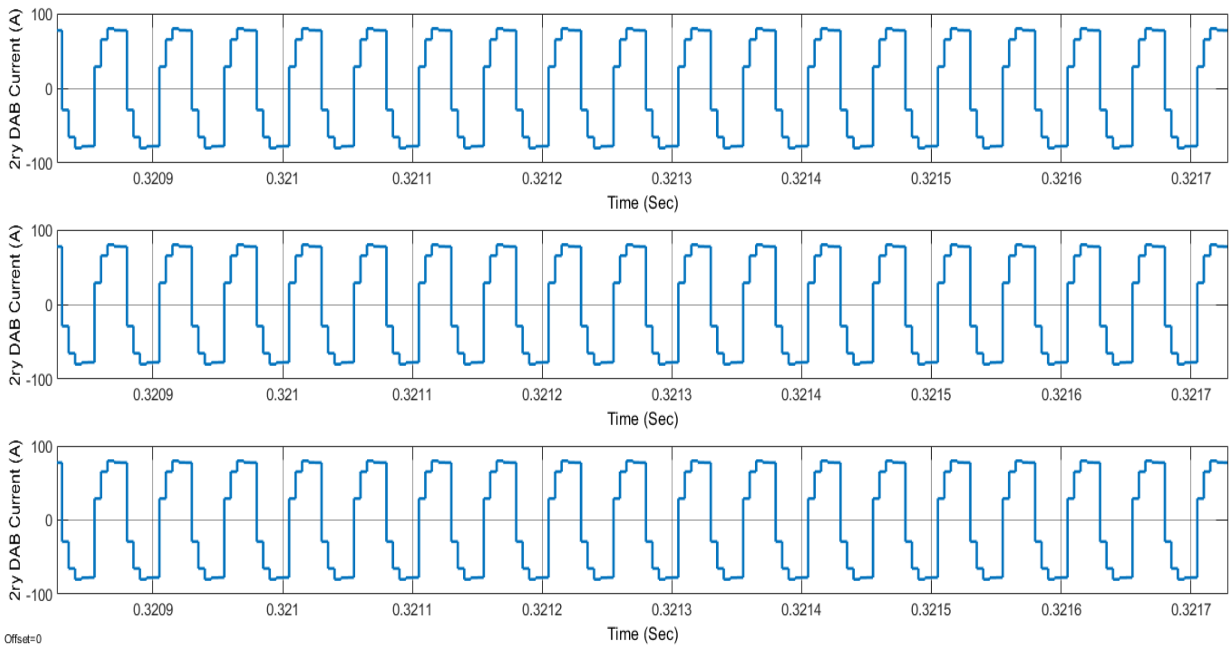

Fig.3.13. Secondary DAB Current

Received: *May 30, 2023;* ***Revised****: 08 October 2023;* ***Accepted:*** *09 October 2023;* ***Published:*** *31 December 2023.*
Corresponding author- ***Yalisho Girma***

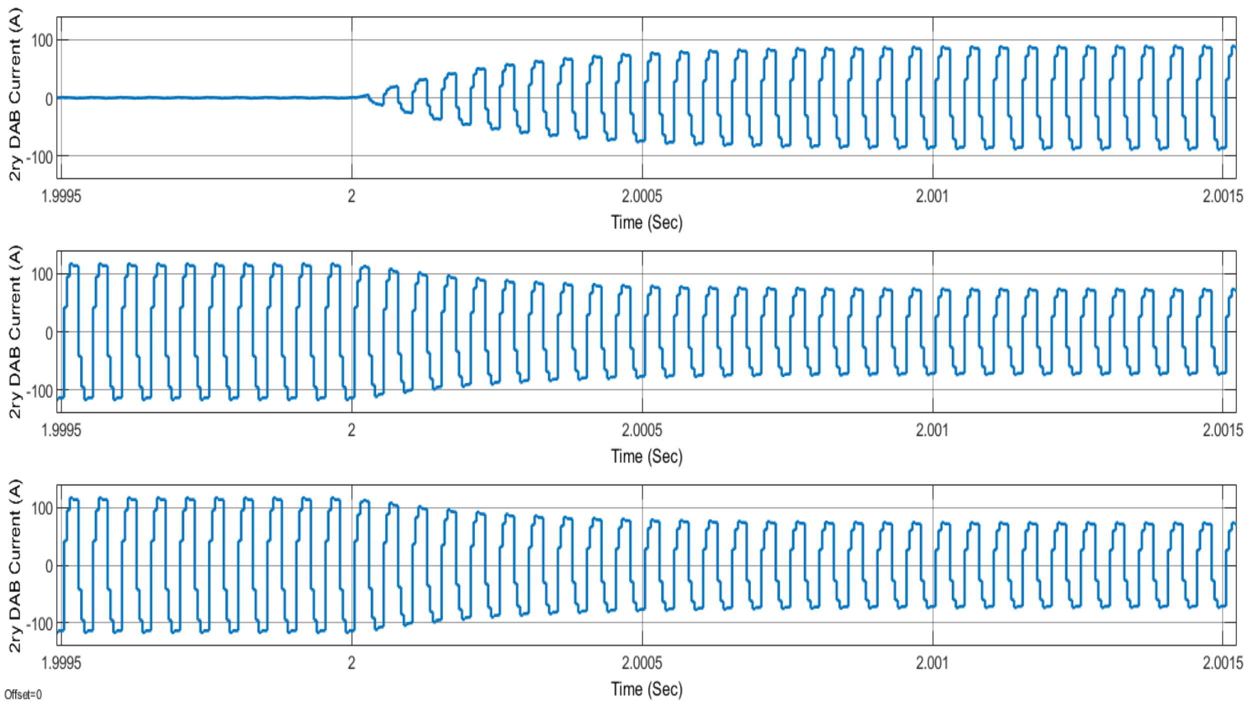

Fig.3.14. Secondary DAB Currents during Fault at DAB_1

Observation: As shown in Fig. 3.12 to Fig. 3.14, the three primary and secondary DABs share the load current equally when all are active. But, when there is a fault in any one of the DABs (secondary DAB in this case), the load current is shared among the un-faulted DABs as shown in Fig.3.14. This fault-tolerant feature of the system is very important in increasing the reliability of the overall system and reducing switching loss during light load conditions.

B. Simulation of Modular Inverter Fed with Solar PV

For simulating the models of modular inverters based on MMC topologies, three three-phase star-connected inductive loads (R-L load) having a maximum demand of 50kVA and a power factor of one (1) are used. Also, a maximum solar irradiance of 800W/m2 and a cell temperature of 45^{0}C is used as an input parameter for the Solar PV array. A steady-state system analysis is used to see changes in output voltage and current.

In Table 4.2 and Table 4.3, the parameter values of the distribution system, converters, and solar PV module are listed. These absolute values were incorporated into the Simulink /PLECS modeling to create the system.

Received: *May 30, 2023;* ***Revised****: 08 October 2023;* ***Accepted:*** *09 October 2023;* ***Published:*** *31 December 2023.*
Corresponding author- ***Yalisho Girma***

Table IV: Technical Specification of Modular Inverter

Parameters	**Value**
Output AC Line Voltage(Vg)	415V
Load resistance (R_L)	3.27 Ω
Load inductance (L_L)	5.5ηH
Maximum Power(S)	50kW
Load Power factor	0.95 to 1 lagging
Sub-module arm inductance (L_arm)	3mH
Sub-module arm resistance (R_arm)	0.1 Ω
Sub-module arm capacitance (C_{SM})	20mF
Capacitance at DC link ($C\_{DC\ Link}$)	10mF
Distribution system frequency(f_g)	50Hz
Carrier frequency (fc)	1000Hz
Modulation index	1
Boost converter duty cycle (D)	0.68
Input DC Voltage to inverter	240V
No of Sub-module per arm (SM)	4

Table V: Technical Specification of Solar PV Array and Its Accessories

Name of Component	**Parameter**	**Value**
	V(open circuit)	85.3V
	V(@Maximum power)	73V
	P_{Max}/Module.	414.8W
	Maximum Irradiation	800kW/cm^2
	Cell temperature	45^{0}C
	Capacity(C_B)	200Ah
	I_{DCH}	0.1C_B
	V(open circuit)	26V

Received: *May 30, 2023;* ***Revised****: 08 October 2023;* ***Accepted:*** *09 October 2023;* ***Published:*** *31 December 2023.*
Corresponding author- ***Yalisho Girma***

ISSN (E): 2959-3921
(P): 2959-393X
DOI: https://doi.org/10.59122/144CFC13

Buck-Boost Converter	Duty cycle	0.11/0.90
	Switching Frequency	5kHz
	Vin/ V_{out}	240V/24V(buck mode)
	Vin/ V_{out}	24V/240V(Boost mode)

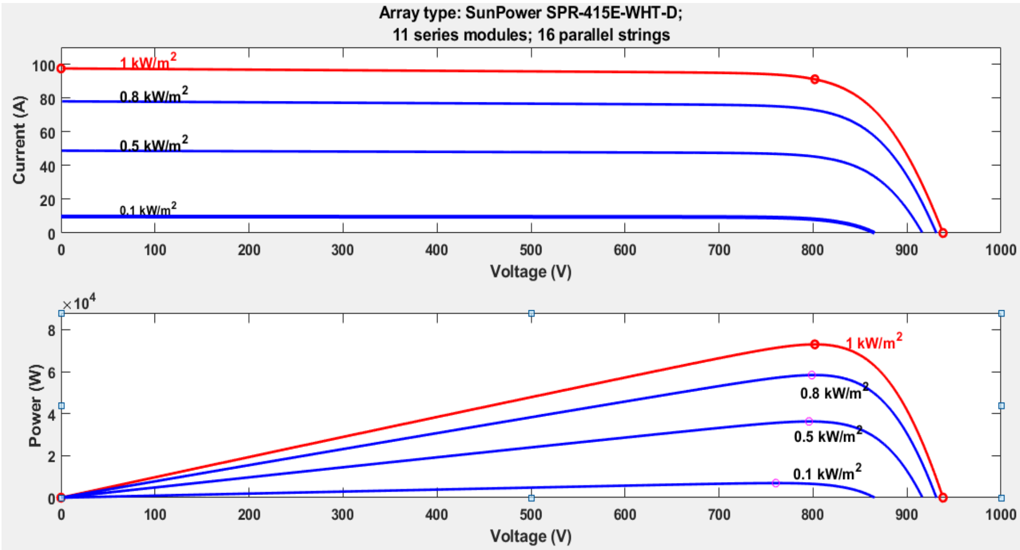

Fig.4.1. Power Versus Voltage and Current Versus Voltage Curve of PV Array

Observation: The PV array supplies the required maximum power demand of 50kW when the solar irradiance is 800w/m^2

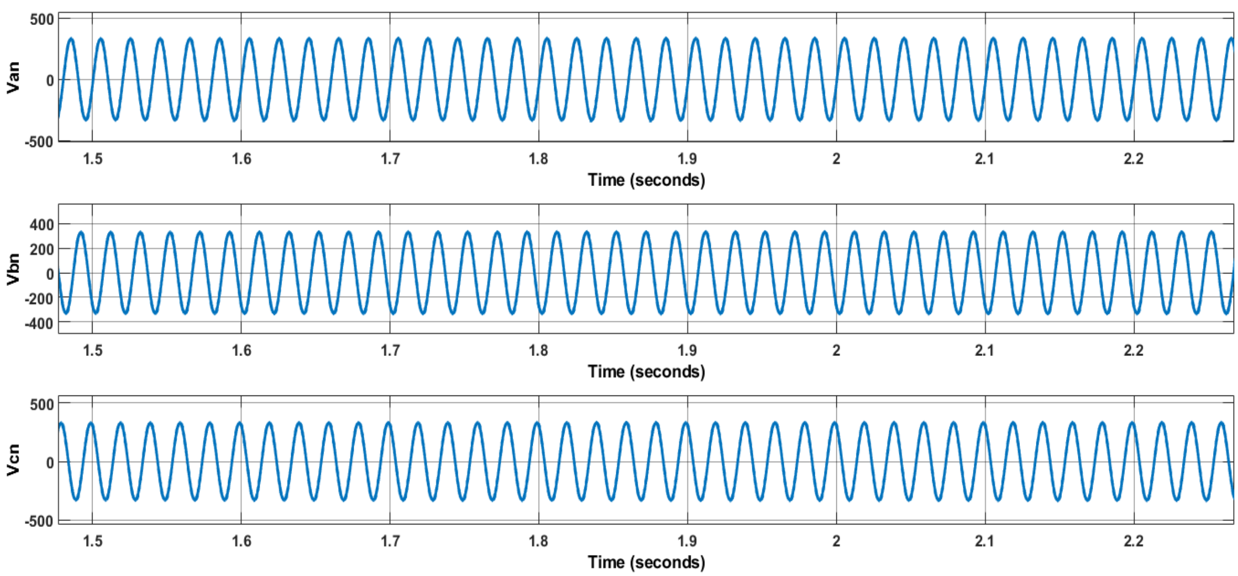

Fig 4.2. Voltage Wave Shape at Modular Inverter Output

Received: *May 30, 2023;* ***Revised****: 08 October 2023;* ***Accepted:*** *09 October 2023;* ***Published:*** *31 December 2023.*
Corresponding author- ***Yalisho Girma***

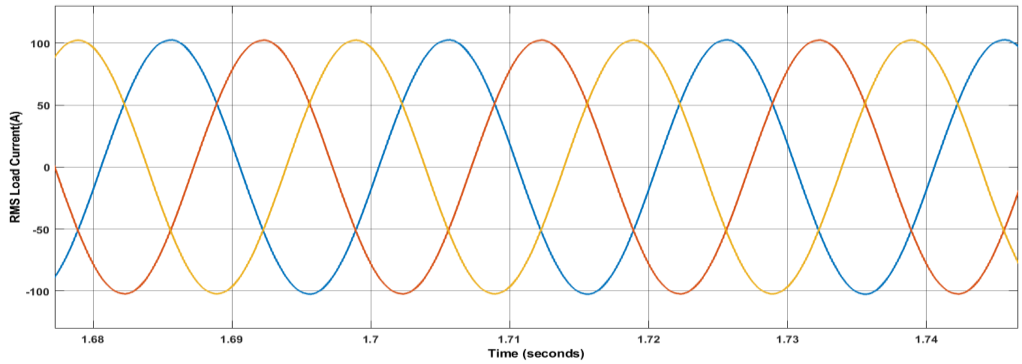

Fig.4.3. Three Phase Load Current Wave Shape of Modular Inverter

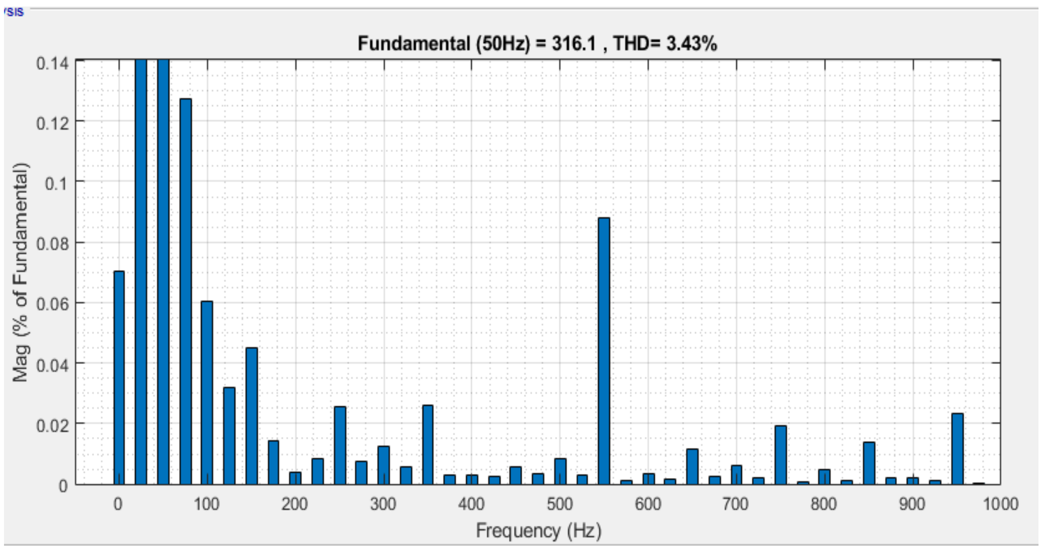

Fig.4.4. Voltage THD at Modular Inverter

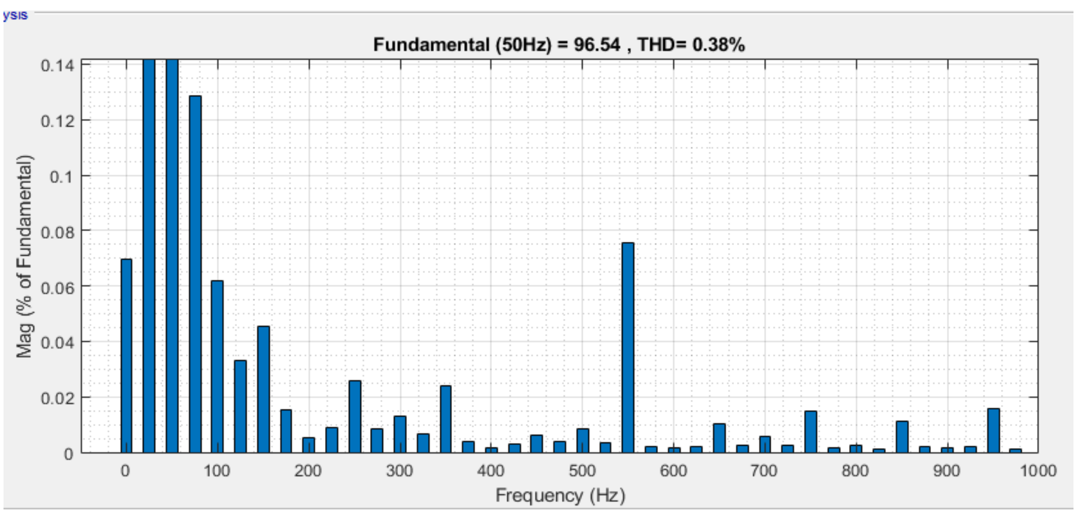

Fig.4.5. Current THD at Modular Inverter Output

Received: *May 30, 2023;* ***Revised****: 08 October 2023;* ***Accepted:*** *09 October 2023;* ***Published:*** *31 December 2023.*
Corresponding author- ***Yalisho Girma***

Observation: As shown in Fig.4.2 to Fig.4.5, the modular inverter output voltage is 230V (PN) when delivering a load current of 73A RMS. Also, the voltage and current THD values are 3.43% and 0.38% respectively, both within the IEEE 519-1992 benchmark. The losses happening in the converter and its achieved efficiency are presented in Table 4 and Fig 4.6 below: -

Table VI: Semiconductor Losses

Device Name	Switching Loss(W)	Conduction Loss (W)	Total Loss (W)	Efficiency (%)
MOSFET	1029.54	818.69	1848.23	96.63

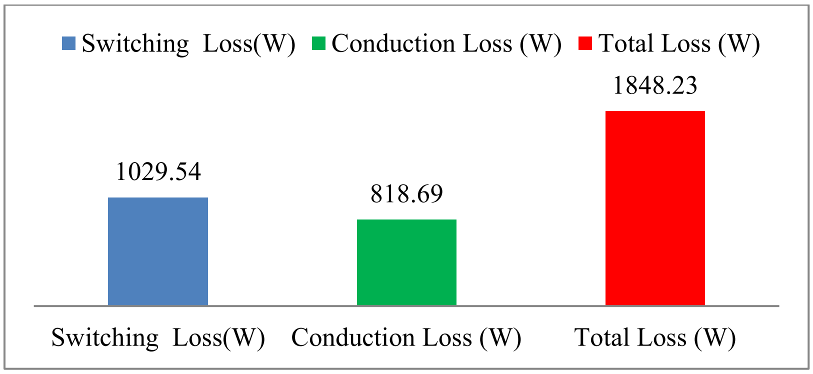

Fig.4.6. Switching and Conduction Losses

Based on the result in Fig.4.6 and equation (27), the efficiency of the system is calculated to be 96.63%.

V. Conclusion

In this research design modeling and technical evaluation of multiport converter-based hybrid power supply for a small village having a maximum demand of 50kW has been done. The multiport converter system contains an isolated DC-DC converter and modular inverter. The isolated DC-DC converter is based on DAB-ISOP configuration whereas the inverter is based on MMC. The DC-DC converter operates at a switching frequency of 20 kHz whereas the modular inverter operates at a switching frequency of 1 kHz. Both converters used a phase-shifted PWM to generate a gating signal. Solar PV array having an output voltage of 240V is used as input to the modular inverter. Also, the system is integrated with battery storage to increase the reliability of the whole system. The battery is charged and discharged through a buck-boost converter having a duty cycle of 0.11(buck mode) and 0.90(boost mode). Simulation results showed that the

Received: *May 30, 2023;* ***Revised****: 08 October 2023;* ***Accepted:*** *09 October 2023;* ***Published:*** *31 December 2023.*
Corresponding author- ***Yalisho Girma***

proposed system is a viable alternative to a low-frequency transformer with many ancillary services such as RES integration and improved availability.

References

[1] M. A. Hannan, P.J. Ker, M. S. Hossain L., Z. H. Choi1, M. S. Abd. Rahman, K. M. Muttaqi, and F. Blaabjerg,“ State of the art of solid-state transformers: Advanced topologies, implementation issues, recent progress and improvements”, *IEEE Access*, vol. 8, pp 19113-19132, Jan. 17, 2020.

[2] L. Wei, L. Gregoire, J. Bélanger, “Control and performance of a modular multilevel converter system,” *CIGRÉ Canada Conf. on Power Systems*, Halifax, Sept. 2011, pp. 1-8.

[3] A. Lesnicar and R. Marquardt, “An innovative modular multilevel converter topology suitable for a wide power range,” *Power Tech Conf. Proceedings, 2003 IEEE Bologna*, Italy, 2003, vol. 3, pp. 1–6.

[4] L. F. Costa, F. Hoffmann, G. Buticchi, and M. Liserre, “Comparative analysis of mab dc-dc converters configurations in modular smart transformer,” *IEEE 8th International Symposium on Power Electronics for Distributed Generation Systems (PEDG)*, April 2017, pp. 1–8. DOI10.1109/PEDG.2017.7972558

[5] M. Hagiwara, K. Nishimura, and H. Akagi, “A medium-voltage motor drive with a modular multilevel PWM inverter,” *IEEE Trans. Power Electron.*, vol. 25, no. 7, pp. 1786–1799, Jul. 2010.

[6] L. Wei, L. Gregoire, J. Bélanger, “Control and performance of a modular multilevel converter system,” *CIGRÉ Canada Conf. on Power Systems*, Halifax, pp. 1-8, Sept. 6-8, 2011.

[7] Y. Zhang, G. P. Adam, T. C. Lim, S.J. Finney, B.W. Williams, “Analysis of modular multilevel converter capacitor voltage balancing based on phase voltage redundant states”, *IET Power Electron*., vol. 5, no. 6, pp. 726–738, July 2012.

[8] Ali Shojaei,” Design of modular multilevel converter-based solid state transformers”, M.S. Thesis, Dept. of Elect. and Compt. Eng., McGill Univ., Montreal, Canada, November 2014.

[9] J. Kolb, F. Kammerer, and M. Braun, "Dimensioning and design of a modular multilevel converter for drive applications," *15th International Power Electronics and Motion Control Conf.* (*EPE/PEMC*), 2012, pp. LS1a-1.1-1-LS1a-1.1-8.

[10] http://www.plexim.com (PLECS User Manual), Jan 14, 2022.

[11] http://www.irt.com/pachage/ (IRFP4668PbF datasheet), Jan 14, 2022.

[12] S. Debdnath, J. Qin, B. Bahrani, M. Saeedifard and P. Barbosa, “Operation, Control, and

Received: *May 30, 2023;* ***Revised****: 08 October 2023;* ***Accepted:*** *09 October 2023;* ***Published:*** *31 December 2023.*

Corresponding author- ***Yalisho Girma***

Applications of the Modular Multilevel Converter: A Review", *IEEE Transactions On Power Electronics*, vol. 30, no. 1, pp. 37-53, Jan. 2015.

[13] S. Rohner, S. Bernet, M. Hiller, and R. Sommer, "Modulation, losses and semiconductor requirements of modular multilevel converters", In *IEEE Transactions on Industrial Electronics*, vol. 57, no. 8, pp. 2633–2642, 2010.

[14] Yalisho Girma, Getachew Biru, Chandra Sekhar "A comparative study on modeling and performances of modular converter based three-phase inverters for smart transformer application", *Journal of Science and Inclusive Development*, vol. 5, no. 2, pp. 91-115, 2023. https://doi.org/10.20372/jsid/2023-256.

[15] T. Kaliannan, J. R. Albert, D. M. Begam and P. Madhumathi, "Power quality improvement in modular multilevel inverter using different multicarrier PWM" *European Journal of Electrical Engineering and Computer Sciences*, vol. 5, no.2, 2023. http://dx.doi.org/10.24018/ejece.2021.5.2.315

[16] M. Park and I.-K. Yu, "A novel real-time simulation technique of photovoltaic generation systems using RTDS," *IEEE Transactions on Energy Conversion*, vol. 19, no. 1, pp. 164–169, 2004.

[17] S. Saravanan, S. Thangavel, "A simple power management scheme with enhanced stability for a solar PV/wind/fuel cell/grid fed hybrid power supply designed for industrial loads", Journal of Electrical and Computer Engineering, vol 2014, Art. ID 319017, 2014. http://dx.doi.org/10.1155/2014/319017

Received: *May 30, 2023;* ***Revised****: 08 October 2023;* ***Accepted:*** *09 October 2023;* ***Published:*** *31 December 2023.*
Corresponding author- ***Yalisho Girma***